

Article

PGE-Enrichment in Magnetite-Bearing Olivine Gabbro: New Observations from the Midcontinent Rift-Related Echo Lake Intrusion in Northern Michigan, USA

Alexander James Koerber and Joyashish Thakurta * 

Department of Geological and Environmental Sciences, Western Michigan University, 1903 W Michigan Ave, Kalamazoo, MI 49008, USA; alexander.j.koerber@wmich.edu

* Correspondence: joyashish.thakurta@wmich.edu; Tel.: +1-(269)-387-3667

Received: 25 November 2018; Accepted: 24 December 2018; Published: 29 December 2018



Abstract: The Echo Lake intrusion in the Upper Peninsula (UP) of Michigan, USA, was formed during the 1.1 Ga Midcontinent Rift event in North America. Troctolite is the predominant rock unit in the intrusion, with interlayered bands of peridotite, mafic pegmatitic rock, olivine gabbro, magnetite-bearing gabbro, and anorthosite. Exploratory drilling has revealed a platinum group element (PGE)-enriched zone within a 45 m thick magnetite-ilmenite-bearing olivine gabbro unit with grades up to 1.2 g/t Pt + Pd and 0.3 wt. % Cu. Fine, disseminated grains of sulfide minerals such as pyrrhotite and chalcopyrite occur in the mineralized interval. Formation of Cu-PGE-rich sulfide minerals might have been caused by sulfide melt saturation in a crystallizing magma, which was triggered by a sudden decrease in fO_2 upon the crystallization and separation of titaniferous magnetite. This PGE-enriched zone is comparable to other well-known reef-like PGE deposits, such as the Sonju Lake deposit in northern Minnesota.

Keywords: Echo Lake; Midcontinent; palladium; platinum; magnetite; gabbro

1. Introduction

Magmatism during the 1.1 Ga old Midcontinent Rift (MCR) event is associated with the origin of several metallic mineral deposits in the Great Lakes region of North America [1–5]. These mineral deposits have been classified into two groups: sulfide-poor, PGE (Platinum Group Element)-rich, layered intrusions and sulfide-rich, conduit-type, high-grade Ni-Cu sulfide deposits (Figure 1) [6,7].

In the first group, several mafic-ultramafic intrusive bodies of the Duluth Complex in northern Minnesota have been identified and studied [3,8,9], which include the Partridge River and South Kawishiwi intrusions, emplaced between 1098 and 1107 Ma [10]. These intrusions are known for basal troctolitic units which host disseminated Cu-Ni-PGE sulfide deposits with ore grades in the following ranges: 0.5–0.7 g/t Pt + Pd + Au; 0.09–0.24 wt. % Ni; 0.27–0.66 wt. % Cu [9]. The Sonju Lake intrusion in the Beaver Bay Complex in northeastern Minnesota shows a PGE-rich interval hosted in an oxide-gabbro unit with precious metallic grades up to Pd: 410 ppb; Pt: 275 ppb and Au: 1.08 ppm [11,12].

The Eagle intrusion, in the Upper Peninsula (UP) of Michigan and the Tamarack intrusion in northeastern Minnesota are the two most important members of the second group. The Eagle Ni-Cu sulfide deposit is hosted within two mafic-ultramafic intrusive bodies, called the Eagle and the Eagle East intrusions, which are associated with the Baraga dike swarm in Marquette County, Michigan [13]. The U-Pb baddeleyite age of the Eagle intrusion is 1107.2 ± 5.7 Ma [13]. The massive, semi-massive, and disseminated sulfide ore deposits in both intrusions are hosted in plagioclase-bearing peridotite,

melanocratic troctolite, and olivine gabbro. The sulfide ore grades are up to 6.11 wt. % Ni and 4.15 wt. % Cu, and up to 25 ppm Pt in Cu-rich stringers [13]. The Tamarack intrusion emplaced during the early stages of the MCR at 1105.6 ± 1.2 Ma [14] is located about 80 km west of the Duluth Complex in Minnesota and it is associated with the Carlton County dike swarm [15]. The funnel-shaped intrusion is composed of peridotite, plagioclase-bearing peridotite, plagioclase-bearing pyroxenite, melanocratic troctolite, and melanocratic gabbro [16]. Massive, semi-massive, and disseminated sulfide-bearing intervals have been identified from drill-core studies with reported drill-intersections of up to 166 m with 2.33 wt. % Ni, 1.24 wt. % Cu, and 0.75 g/t Pt + Pd + Au [16].

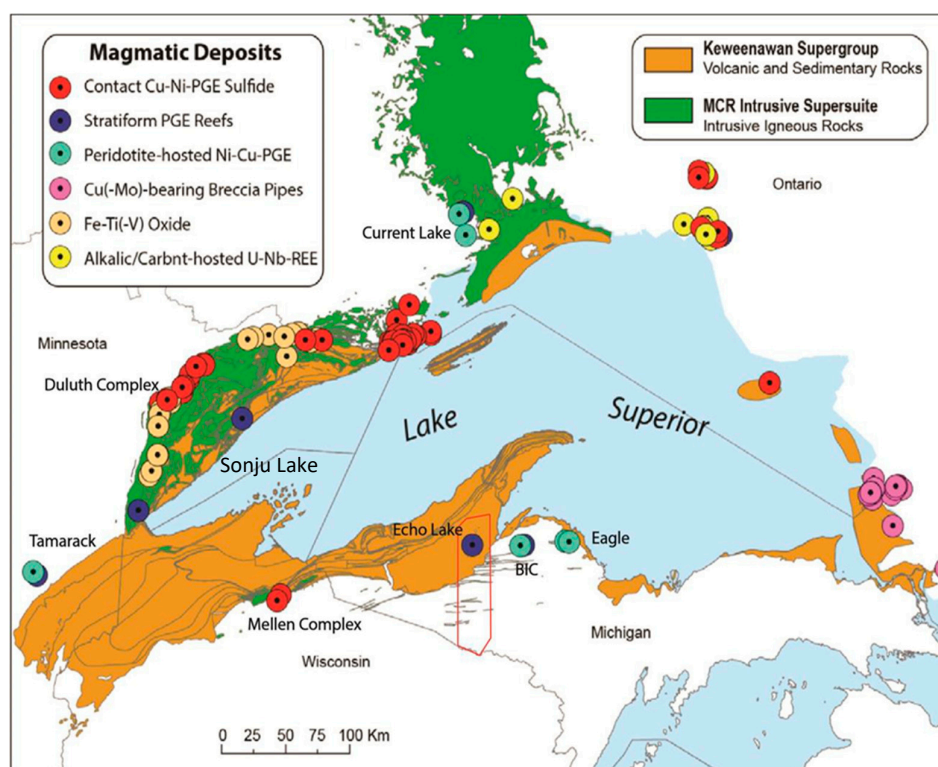


Figure 1. Magmatic ore deposits associated with the Midcontinent Rift around Lake Superior. The red box shows the location and extent of the exploration prospect zone called the Voyageur Lands [6,7].

This study is focused on the newly discovered Echo Lake intrusion, located in the Houghton and Ontonagon counties in UP Michigan (Figures 1 and 2) [17]. Exploratory drilling has identified this intrusion as a new prospect for sulfide mineralization in the Midcontinent Rift region [18]. The basement rock in the area of the intrusion is an Archean granite-gneiss [19], which is overlain by the Paleoproterozoic Michigamme Formation [20]. The latter consists of meta-greywacke, slate, metamorphosed mafic volcanics, and iron formations. The 1110 Ma Mesoproterozoic Siemens Creek Volcanics unit [1] unconformably overlies the Michigamme Formation. The Neoproterozoic Jacobsville Formation [21] overlies both the Siemens Creek Volcanics unit and the Michigamme Formation. The uppermost layer of the Echo Lake intrusion has been encountered by drill-cores at about 200 m underneath the Jacobsville Formation, and it is estimated to extend laterally for about 18 square kilometers [18]. The complete thickness of this intrusion is unknown at this stage, but a continuous succession of mafic-ultramafic rocks for more than 1 km has been reported. Being located between the Keweenaw and the Marenisco regional faults [17], the Echo Lake intrusion might have been uplifted from greater depths by displacements along these two faults. Apart from Echo Lake, there are several other small outcrops of mafic-ultramafic bodies in the area, such as the Bluff, Haystack, and Skinny intrusions (Figure 2) [22], which are mostly composed of gabbro, gabbro-norite, and pyroxenite. The ages and mutual relationships of these intrusions are unknown.

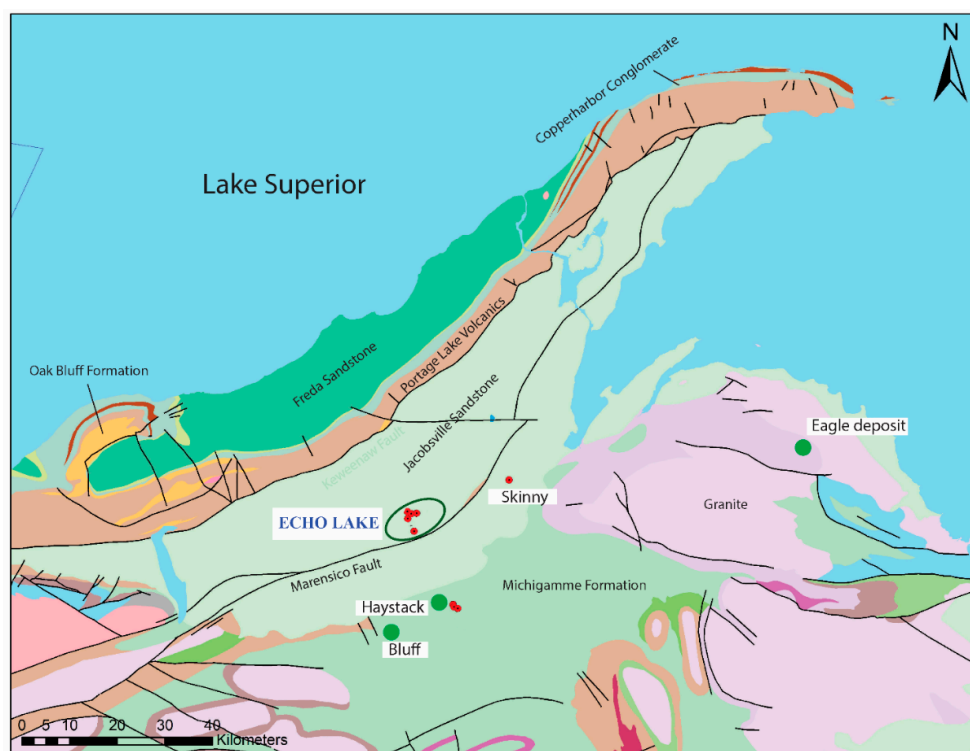


Figure 2. Location of Echo Lake prospect in the Upper Peninsula of Michigan, near the southern shore of Lake Superior [17]. Green circles indicate a few other metal prospects and mines in the area. Red circles indicate drill core locations.

The Echo Lake intrusion has been dated at 1111 Ma [23], which makes it contemporaneous with the Early Rift-forming phase of the MCR. Troctolite is the predominant rock in the intrusion, but recurrent layers of peridotite, mafic pegmatitic rock, olivine- and magnetite-bearing gabbro, and anorthosite have also been documented. This is comparable with the rhythmic layering reported from the Duluth Complex and other layered mafic-ultramafic complexes around the world, such as the Bushveld in South Africa [24] and Stillwater, in Montana, USA [25,26]. Our aims in the present study are to examine the PGE-enriched zone in the Echo Lake intrusion. Petrological analysis, along with whole rock and mineral compositional data, were used to highlight key characteristics of the Echo Lake intrusion and to compare them with the known sulfide-mineralized intrusions in the MCR.

2. Methods

For this study, one hundred and seventy samples were collected from drill cores EL-1, EL-97-05, EL-97-03, and 10EL-001 in the core repositories of Altius Resources Inc. (St. John's, NL, Canada) and the Department of Environmental Quality, Michigan.

Electron microprobe analysis (EMPA) was performed at the Department of Geoscience, University of Wisconsin-Madison, USA, using a 5-spectrometer, CAMECA SX5 electron microprobe (CAMECA, Gennevilliers, France). The probe was operated at 15 kV with a beam Faraday cup current of 20 nA and beam size of two microns. Analytical standards are both natural and synthetic silicate minerals, glasses, and oxides. Counting times were 10 s on peak. Background intensities were determined by the mean atomic number background algorithm [27].

Bulk rock chemical analyses were performed at Geoscience Laboratories in Sudbury, Ontario, Canada. Inductively Coupled Plasma Mass Spectrometer (ICP-MS) technique was used to analyze for Ni, Cu, PGE and Au. Sample analytes were prepared using fire-assay and closed vessel acid-digestion methods.

3. Results

Troctolite and olivine gabbro are the two dominant rock types in the intrusion. Troctolite samples are typically composed of 60 vol. % plagioclase, 30 vol. % olivine, 5% vol. % pyroxene, minor Fe-Ti oxides, traces of biotite and sulfide minerals such as pyrrhotite, chalcopyrite, and pentlandite (Figure 3A,B). Olivine gabbro samples are typically composed of about 50% olivine, 30% plagioclase, 10–15% pyroxene, 5–10% Fe-Ti oxides, and traces of sulfide minerals. Sulfide minerals in troctolite and olivine gabbro samples are disseminated grains of pyrrhotite, chalcopyrite, and pentlandite which form mutual intergrowths with one another (Figure 3B). Traces of other sulfide minerals, like digenite and bornite, have also been found. Sulfide minerals often form thin rims around titaniferous magnetite and ilmenite crystals (Figure 4C). Titaniferous magnetite occurs as intergrowths with biotite (Figure 4A). Titaniferous magnetite also shows delicate intergrowths and reaction textures with sulfide minerals (Figure 4B,C).

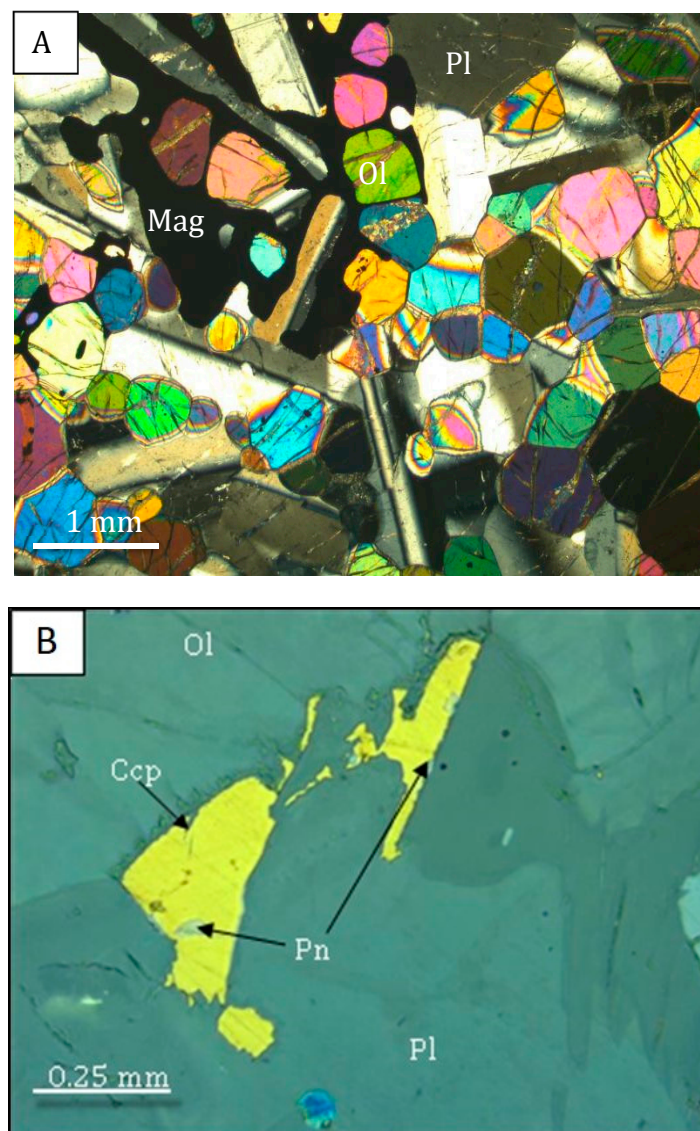


Figure 3. Troctolite showing: (A) Intergranular texture between plagioclase and olivine (Ol). Interstitial titaniferous magnetite (Mag) is seen surrounding grains of plagioclase (Pl) and olivine (transmitted light); (B) Fine intergrowths of chalcopyrite (Ccp) and pentlandite (Pn) in the interstices of olivine and plagioclase (reflected light). The blue hexagonal grain at the bottom is digenite.

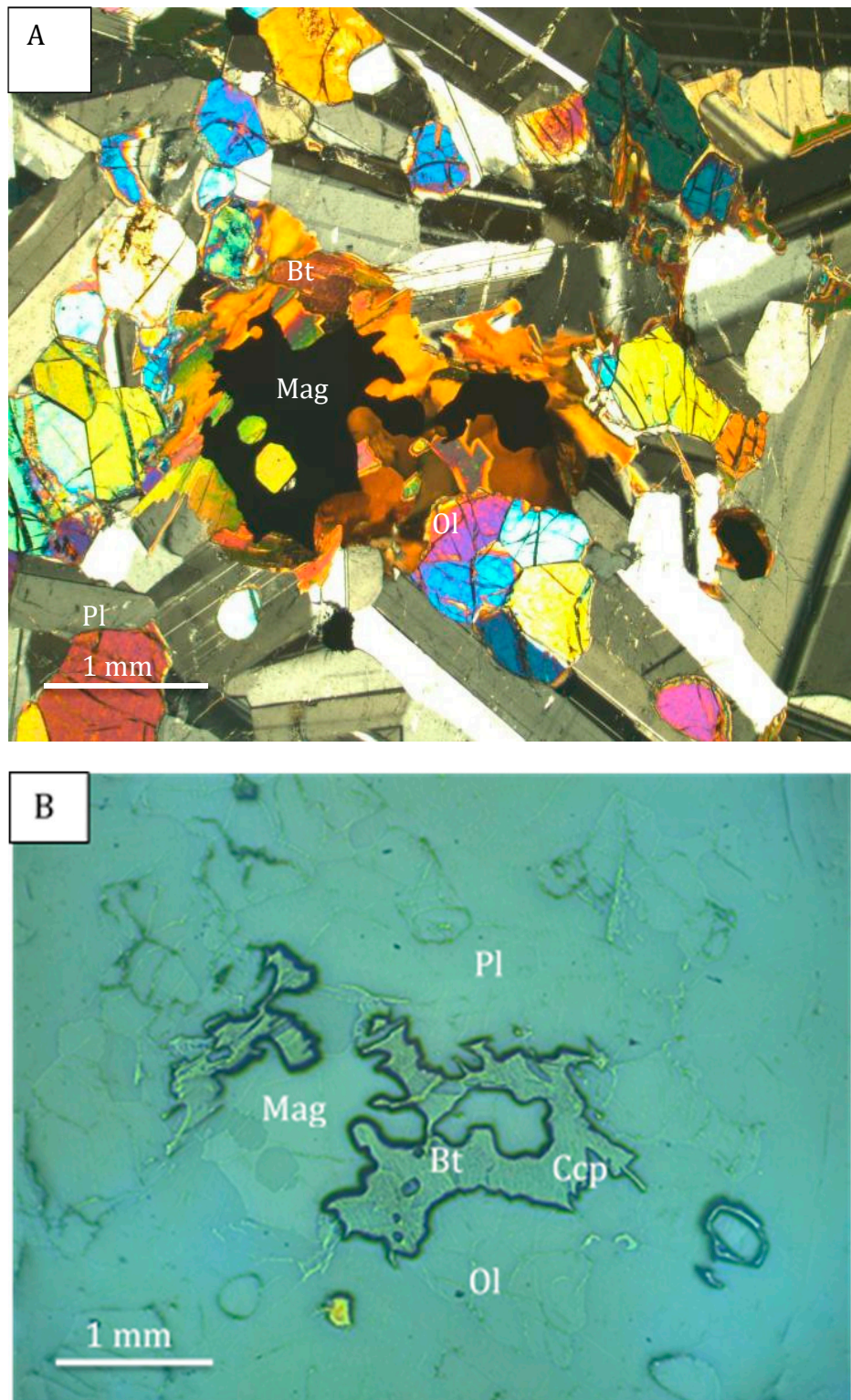


Figure 4. Cont.

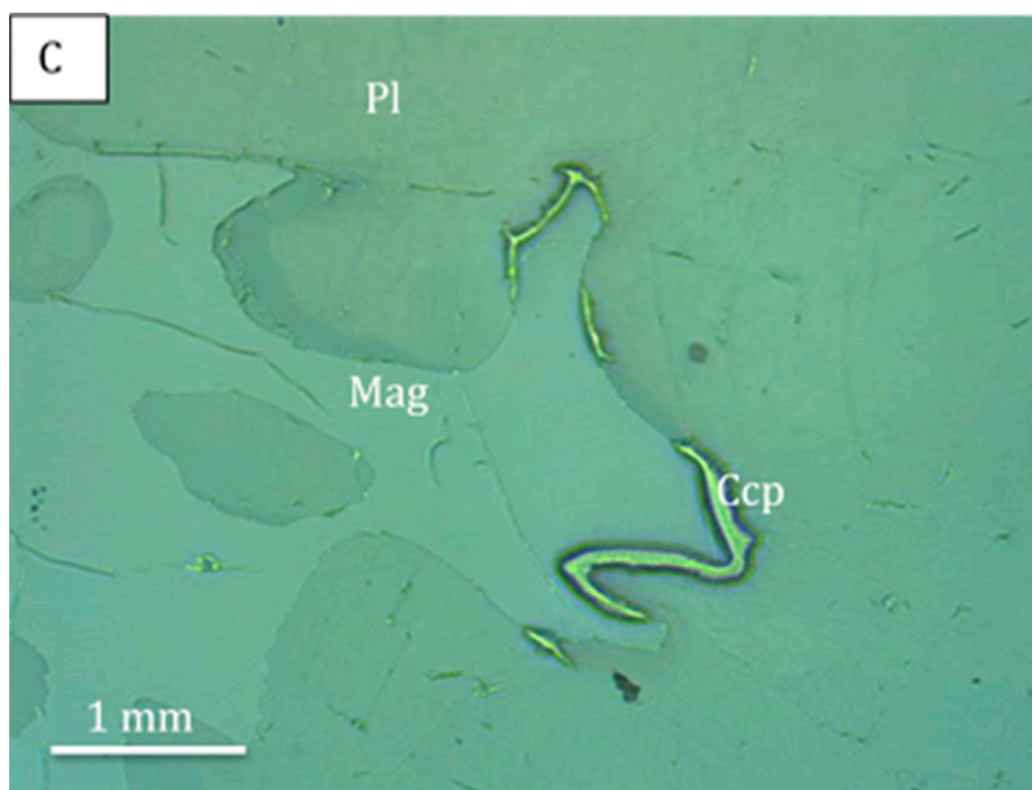


Figure 4. Magnetite-bearing olivine gabbro showing: (A) Cumulus texture in plagioclase and olivine with biotite (Bt)-magnetite (Mag) intergrowth in small interstitial spaces (transmitted light); (B) Biotite-magnetite intergrowth and fine disseminated chalcopyrite (reflected light); (C) Thin rim of chalcopyrite (Ccp) around titaniferous magnetite (Mag) in contact with plagioclase (Pl).

A stratigraphic sequence of the observed layered units in the Echo Lake intrusion, as revealed from drill core studies, is shown in Figures 5–7. Notable PGE-enrichment is observed within a 45 m thick layer of Fe-Ti oxide rich olivine gabbro. Titaniferous magnetite and ilmenite are the principal oxide minerals. These minerals mostly constitute 10–25 vol. % of the oxide-rich olivine gabbro unit. However, in some parts, the oxide minerals form massive zones with fine interstitial grains of silicate minerals (Figure 4). At the Fe-Ti oxide-rich zone, there is an interval with disseminated grains of sulfide minerals. Peak concentrations of Pt and Pd of 550 ppb and 634 ppb, respectively, are measured in this interval at a depth of about 998 m [18]. Pt and Pd contents show positive correlation in all studied depths of the intrusion, although Pd shows a higher concentration in most intervals (Figures 5 and 6). Stratigraphic variations of MgO, TiO₂, Cr₂O₃, and FeO (total) in the layered sequences are shown in Figure 8.

The whole-rock major element compositions of the major rock-types are shown in Table 1. Compositions of olivine, clinopyroxene, plagioclase, and titaniferous magnetite in the major rock types are shown in Tables 2–5. Olivine composition in the troctolite units of the Echo Lake intrusion shows a range between Fo_{57–62}. Clinopyroxene in these rocks plot within the compositional range of augite (Table 3). Plagioclase compositions range between An_{55–75} (Table 4). The Cr₂O₃-content of titaniferous magnetite in most intervals is about 3 wt. % (Table 5), although in some local intervals a Cr₂O₃ content above 9 wt. % is seen. The TiO₂-content in titaniferous magnetite in troctolite and olivine gabbro ranges between 7 and 10 wt. %, but in olivine-magnetite gabbro it ranges between 12 and 18 wt. %. The high TiO₂-content in magnetite is indicative of the possible existence of fine exsolution lamellae of ulvöspinel.

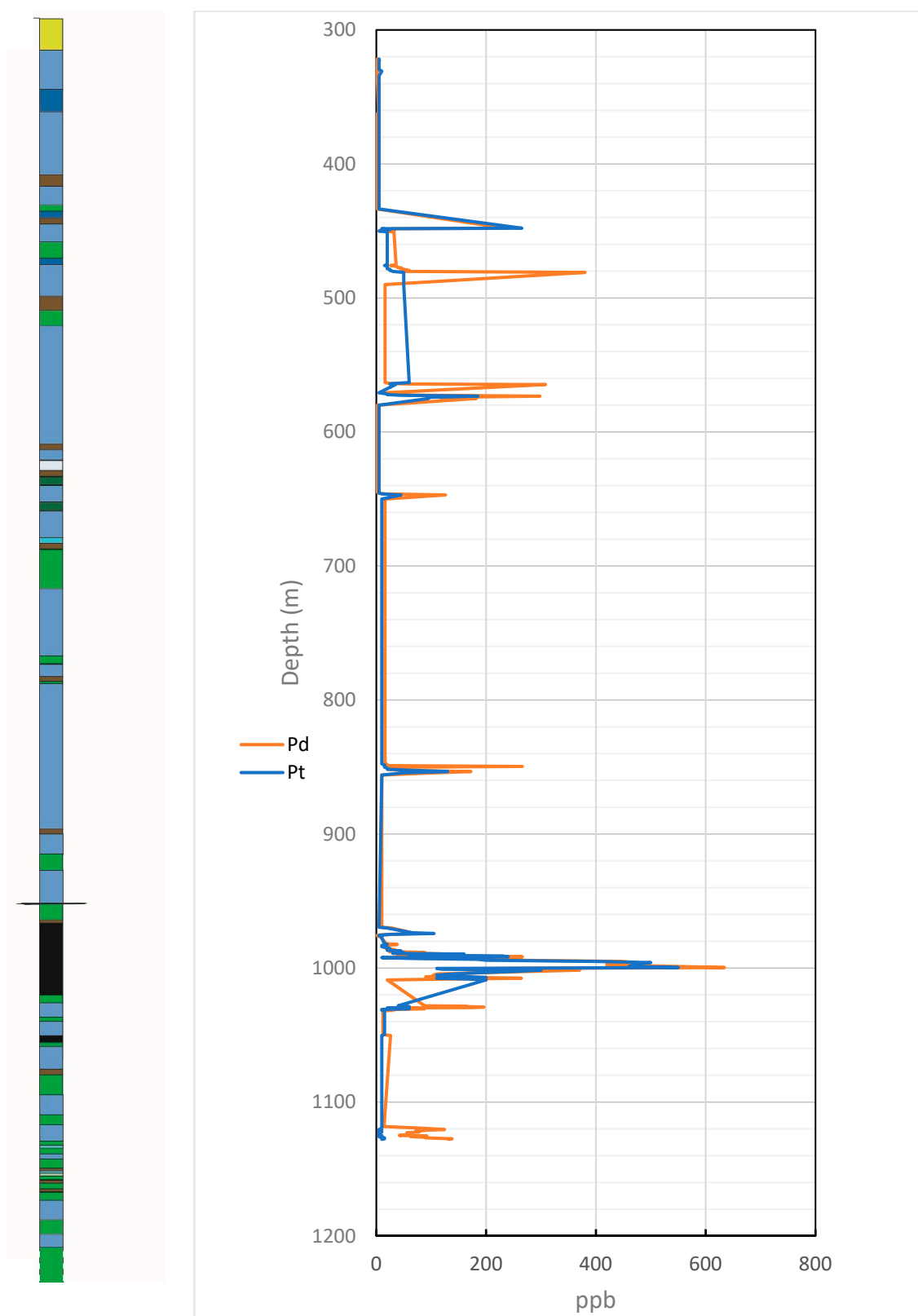


Figure 5. The layered ultramafic-mafic succession observed in the Echo Lake intrusion and locations of the zones of platinum group element (PGE)-enrichment in the intrusion. The magnetite-bearing olivine gabbro shows peak concentrations. The most highly mineralized interval between 970 m and 1050 m has been expanded in Figure 6.

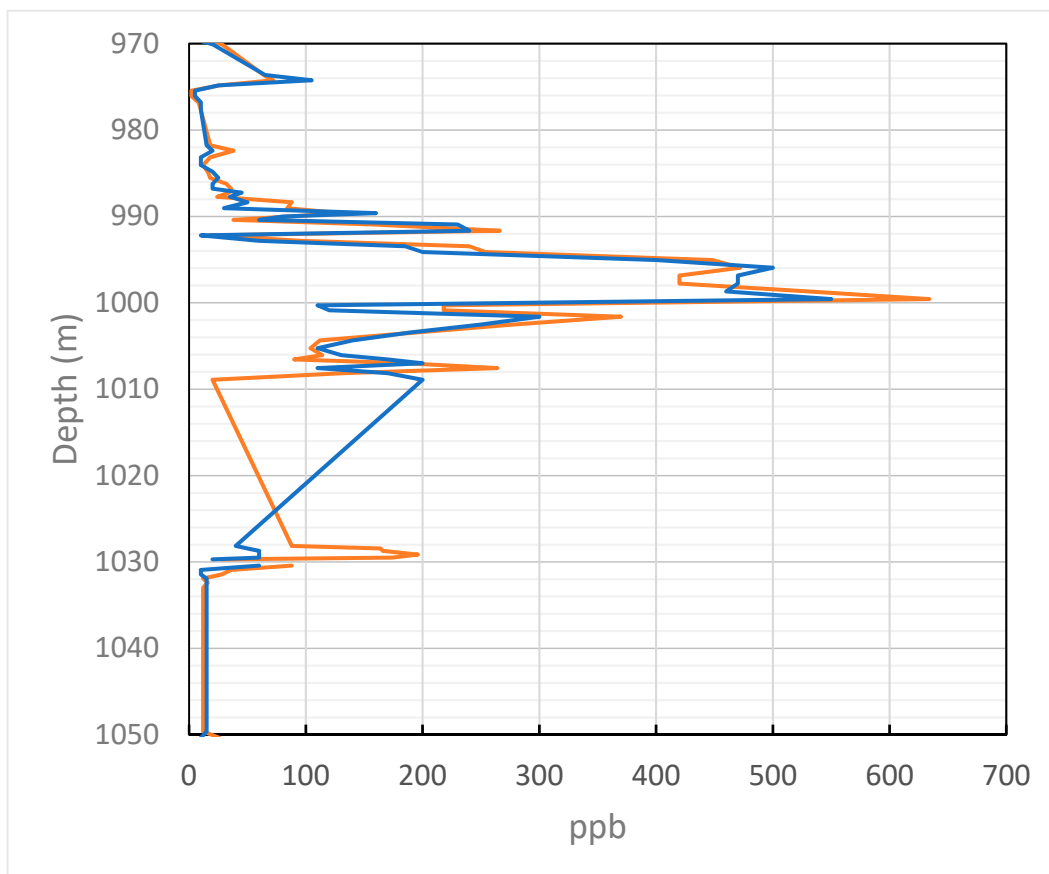


Figure 6. PGE concentrations in the mineralized zone.

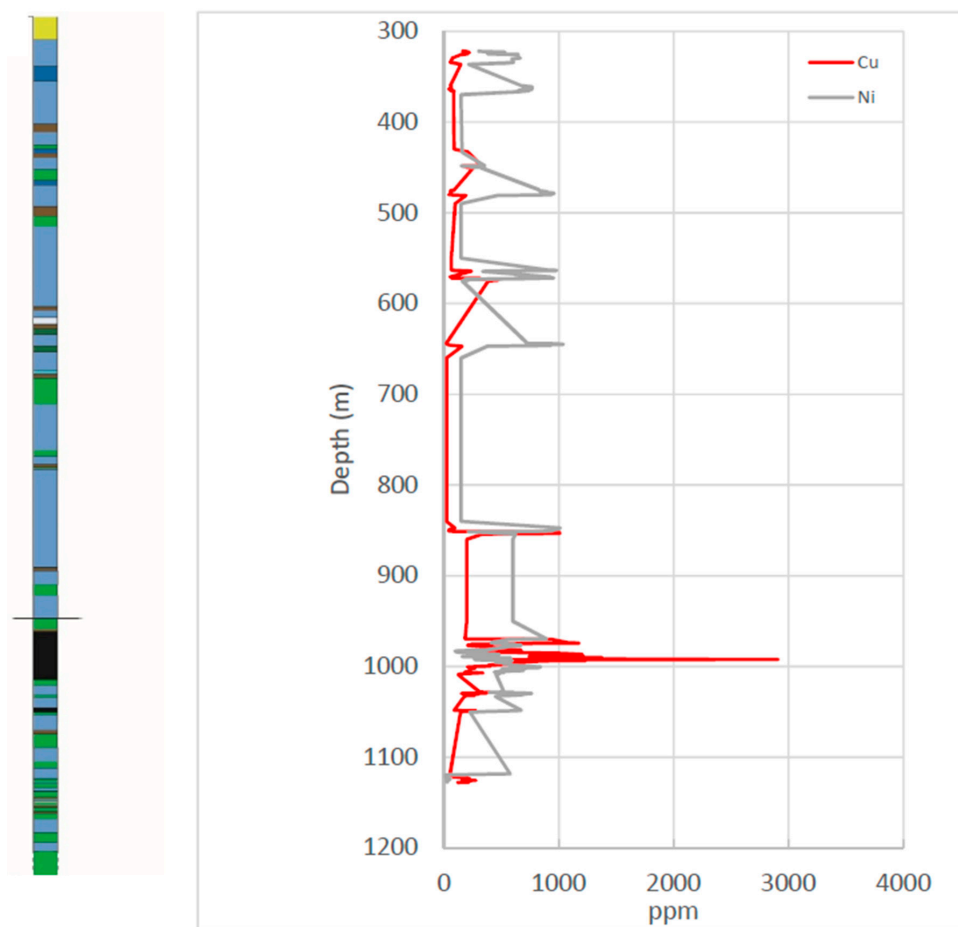


Figure 7. Concentrations of Cu and Ni in the layered succession.

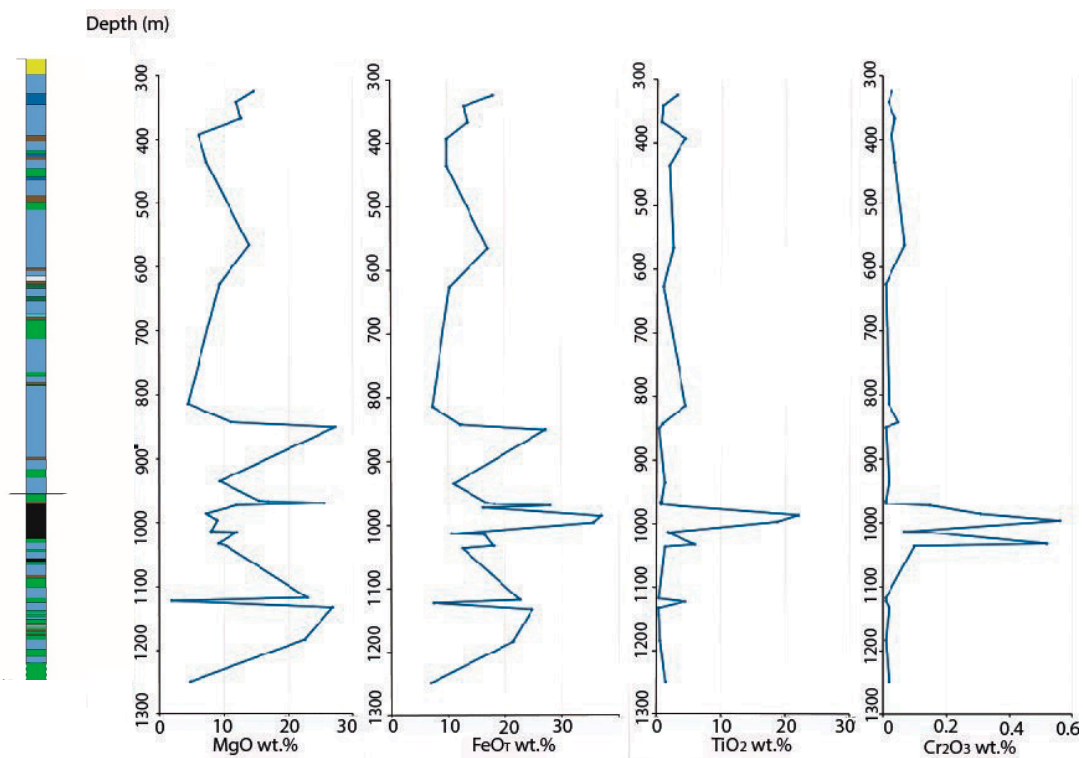


Figure 8. Stratigraphic variation plots of MgO, TiO₂, FeO_T, and Cr₂O₃.

Table 1. Major element compositions of principal rock types.

Drill Core	EL9703	10EL001	EL9703	EL9703	EL9703	EL9703	10EL001	EL9703	EL9703
Rock Type	Trt	Trt	Trt	Trt	Trt	Trt	Trt	Trt	Trt
Depth (m)	325.5	393.0	436.2	565.7	626.4	842.8	814.1	966.8	1015.0
SiO ₂	43.50	48.47	46.83	43.50	47.01	45.70	49.69	42.80	43.60
TiO ₂	1.45	2.15	0.90	1.21	0.47	0.44	2.20	0.28	0.93
Al ₂ O ₃	12.30	18.75	21.55	13.90	20.60	18.10	21.23	12.60	16.35
Cr ₂ O ₃	0.03	0.03	0.04	0.07	0.01	0.05	0.02	0.01	0.14
Fe ₂ O ₃	19.90	11.00	11.01	18.90	11.52	13.50	8.07	20.10	18.20
FeO	17.91	9.90	9.91	17.01	10.37	12.15	7.26	18.09	16.38
MnO	0.22	0.15	0.12	0.20	0.13	0.14	0.11	0.22	0.18
MgO	14.60	6.13	7.40	13.90	9.36	11.10	4.46	16.90	12.05
CaO	6.24	9.71	9.61	6.38	9.07	8.29	11.30	5.80	7.23
Na ₂ O	1.79	2.74	2.79	2.00	2.70	2.34	3.10	1.70	2.38
K ₂ O	0.33	0.66	0.31	0.31	0.26	0.18	0.51	0.14	0.21
P ₂ O ₅	0.15	0.27	0.07	0.14	0.06	0.03	0.07	0.03	0.02
TOTAL	99.60	100.56	100.55	99.40	100.85	99.60	100.98	99.40	100.20
Drill Core	8412	EL9703	EL9703	8413	8414	EL9703	EL9703	10EL001	EL9703
Rock Type	Mt-Ol-gab	Mt-Ol-gab	Mt-Ol-gab	Ol-gab	Ol-gab	Ol-gab	Ol-gab	Ol-gab	Ol-gab
Depth (m)	935.4	965.6	972.9	1013.8	1032.7	1036.3	1122.6	1248.3	1183.5
SiO ₂	45.80	44.03	45.40	47.10	41.80	45.80	48.50	48.04	40.60
TiO ₂	0.60	0.35	1.83	0.85	2.92	0.63	2.20	0.68	0.25
Al ₂ O ₃	21.29	14.73	11.90	19.40	15.25	18.30	21.50	23.93	8.64
Cr ₂ O ₃	0.02	0.01	0.15	0.07	0.52	0.10	0.01	0.02	0.01
Fe ₂ O ₃	12.24	18.79	18.00	11.80	19.90	13.90	8.25	7.62	23.70
FeO	11.01	16.91	16.20	10.62	17.91	12.51	7.42	6.86	21.33
MnO	0.14	0.21	0.21	0.13	0.19	0.14	0.09	0.10	0.25
MgO	9.40	15.36	12.00	8.06	9.18	10.30	1.98	4.80	22.50
CaO	8.79	6.50	9.64	9.14	8.38	8.06	11.40	10.43	3.91
Na ₂ O	2.54	1.93	1.59	2.67	2.24	2.49	3.26	3.00	1.10
K ₂ O	0.32	0.19	0.17	0.25	0.26	0.19	0.47	0.37	0.10
P ₂ O ₅	0.08	0.03	0.07	0.03	0.04	0.03	0.32	0.06	0.03
TOTAL	100.92	100.98	100.30	99.20	99.73	99.30	98.40	100.75	100.40

Trt = troctolite; Ol-gab = olivine gabbro; Mt-Ol-gab = magnetite-bearing olivine gabbro.

Table 2. Composition of olivine in the major rock types.

Drill Core	EL9703	EL9703	EL9703	EL9703	10EL001	EL9703	EL9703
Rock Type	Trt	Trt	Ol-gab	Ol-gab	Ol-gab	Mt-Ol-gab	Mt-Ol-gab
Depth (m)	440.2	440.2	935.5	1008.91	1158.4	992.64	985.7
SiO ₂	35.09	36.44	35.85	35.62	36.68	35.60	35.79
FeO	33.20	33.25	33.43	34.55	34.48	35.46	33.36
MnO	0.45	0.43	0.46	0.45	0.47	0.44	0.38
MgO	30.29	30.41	29.91	29.30	28.76	28.72	30.43
NiO	0.13	0.09	0.12	0.12	0.07	0.11	0.03
CaO	0.06	0.05	0.03	0.06	0.04	0.10	0.08
TOTAL	99.23	100.66	99.79	100.09	100.50	100.43	100.06
Normalized to 4 oxygens							
Si	0.97	1.01	0.98	0.99	1.01	0.99	0.99
Fe(2+)	0.77	0.77	0.77	0.81	0.80	0.83	0.77
Mn	0.01	0.01	0.01	0.01	0.01	0.01	0.01
Mg	1.25	1.25	1.22	1.22	1.18	1.20	1.26
TOTAL	3.00	3.05	2.98	3.04	3.01	3.03	3.04
Fo (mol %)	61.6	61.7	61.1	59.9	59.5	58.8	61.7
Ni (ppm)	1060.7	739.9	950.1	926.0	575.0	838.5	259.0

Table 3. Composition of clinopyroxene in the major rock types.

Drill Core	EL9703	EL9703	EL9703	EL9703	EL9703	10EL001
Rock Type	Trt	Trt	Ol-gab	Mt-gab	Ol-gab	Ol-gab
Depth (m)	440.22	440.22	935.52	985.76	1008.91	1158.4
SiO ₂	51.06	51.31	51.85	51.45	51.22	51.20
TiO ₂	0.86	0.85	0.96	1.15	1.08	0.95
Al ₂ O ₃	2.13	2.28	2.59	2.57	2.34	2.42
Cr ₂ O ₃	0.11	0.13	0.07	0.13	0.11	0.06
FeO _(total)	9.26	10.07	9.45	10.96	9.91	9.57
MnO	0.24	0.25	0.23	0.28	0.24	0.24
MgO	14.80	15.66	14.67	14.12	14.35	14.33
CaO	20.73	19.02	20.69	19.72	20.78	21.31
Na ₂ O	0.27	0.23	0.32	0.28	0.28	0.31
TOTAL	99.49	99.83	100.84	100.66	100.32	100.43
Normalized to 6 oxygens						
Si	1.91	1.92	1.94	1.92	1.91	1.91
Al	0.09	0.10	0.11	0.11	0.10	0.11
Cr	0.00	0.00	0.00	0.00	0.00	0.00
Fe(3+)	0.01	0.06	0.16	0.06	0.06	0.09
Fe(2+)	0.28	0.25	0.14	0.28	0.25	0.21
Ti	0.02	0.02	0.03	0.03	0.03	0.03
Mn	0.01	0.01	0.01	0.01	0.01	0.01
Mg	0.82	0.87	0.82	0.79	0.80	0.80
Ca	0.83	0.76	0.83	0.79	0.83	0.85
Na	0.02	0.02	0.02	0.02	0.02	0.02
TOTAL	4.00	4.02	4.05	4.02	4.02	4.03
Wo	42.1	38.6	42.0	40.5	42.3	43.1
En	41.8	44.2	41.5	40.4	40.6	40.3
Fs	15.1	16.3	15.3	18.0	16.1	15.5
Ae	1.0	0.9	1.2	1.0	1.0	1.1

Table 4. Composition of plagioclase in the major rock types.

Drill Core	EL9703	EL9703	EL9703	EL9703
Rock Type	Trt	Trt	Mt-Ol-gab	Ol-gab
Depth (m)	440.2	440.2	985.76	1008.91
SiO ₂	54.15	51.66	53.50	53.56
Al ₂ O ₃	28.50	31.09	29.73	29.49
FeO	0.33	0.47	0.26	0.48
CaO	11.38	13.64	11.78	11.91
Na ₂ O	4.82	2.29	4.77	4.48
K ₂ O	0.41	0.39	0.33	0.45
TOTAL	99.59	99.54	100.37	100.36
Normalized to 8 oxygens				
Si	9.81	9.36	9.69	9.70
Al	6.08	6.64	6.35	6.30
Fe (2+)	0.05	0.07	0.04	0.07
Ca	2.21	2.65	2.29	2.31
Na	1.69	0.80	1.68	1.57
K	0.10	0.09	0.08	0.10
TOTAL	19.94	19.61	20.12	20.06
An	55.3	74.7	56.6	58.0
Ab	42.4	22.7	41.5	39.4
Or	2.4	2.4	1.9	2.6

Table 5. Composition of titaniferous magnetite in major rock types.

Drill Core	EL97-03	EL-97-03	EL-97-03	EL-97-03	10EL001	10EL001
Rock Type	Ol-gab	Mt-gab	Mt-gab	Trt	Ol-gab	Ol-gab
Depth (m)	980.67	985.40	984.4	440.2	968.96	1158.4
TiO ₂	5.66	17.38	15.98	8.32	7.01	5.44
Al ₂ O ₃	3.88	3.76	4.27	5.45	3.87	2.21
FeO tot	84.62	74.02	73.21	75.01	83.70	88.44
Fe ₂ O ₃ (calc)	49.87	29.19	29.80	37.56	47.66	53.15
FeO (calc)	34.76	44.82	43.40	37.45	36.05	35.29
MnO	0.30	0.32	0.38	0.41	0.26	0.27
MgO	1.12	1.67	1.72	1.25	1.12	0.56
Cr ₂ O ₃	3.42	2.19	3.37	9.29	3.23	2.73
TOTAL	99.00	99.34	98.93	99.73	99.18	99.65
Normalized with respect to 3 cations						
Ti	0.15	0.47	0.43	0.22	0.19	0.15
Al	0.16	0.16	0.18	0.23	0.16	0.09
Fe(3+)	1.44	0.85	0.86	1.07	1.37	1.54
Fe(2+)	1.08	1.37	1.33	1.14	1.12	1.11
Mn	0.01	0.01	0.01	0.01	0.01	0.01
Mg	0.06	0.09	0.09	0.07	0.06	0.03
Cr	0.10	0.06	0.10	0.26	0.09	0.08
TOTAL	3.00	3.00	3.00	3.00	3.00	3.00

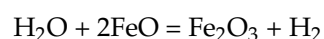
4. Discussion

In this section the PGE-enrichment reported from the Echo Lake intrusion is discussed with reference to the geochemical principles of sulfide-melt saturation in basaltic and picritic magmas. These discussions are then placed in the context of economic mineral deposits in igneous intrusive bodies associated with the Midcontinent Rift.

4.1. Sulfide-Melt Saturation in Basaltic and Picritic Magmas

Sulfur is an incompatible element during crystallization of silicate minerals, and thus it can remain dissolved in magma until a late stage of crystallization. Sulfur concentration in magma can increase by mechanisms such as fractional crystallization and the assimilation of sulfur from external sources [28–31]. Upon the attainment of sulfide liquid saturation, an immiscible sulfide liquid is formed from the magma, which sequesters chalcophile elements such as Cu, Ni, and PGE. For most S-rich Ni-Cu deposits, such as Eagle [32] and Tamarack [33], incorporation of external sulfur is regarded as an essential requirement to attain sulfide liquid saturation [31]. However, for sulfur-poor PGE deposits, such as the Partridge River and South Kawishiwi intrusions in the Duluth Complex, prolonged fractional crystallization of magma has been proposed as an effective mechanism to induce sulfide liquid saturation [5,31].

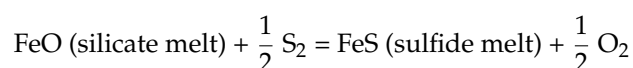
Sulfide liquid saturation is also strongly influenced by fO_2 [34,35] and the solubility of sulfur in the magma can be inversely correlated with the Fe^{2+} content. Prolonged fractional crystallization in a closed system is one mechanism for increasing the fO_2 of the magma. Early fractionations of anhydrous minerals such as olivine, plagioclase, and pyroxene in a closed system can increase the mole fraction of dissolved H_2O in the magma [36]. In an open system, H_2O -content of the magma can be increased by assimilation of hydrous country rocks [37,38]. These factors can cause higher oxygen availability, and thus cause higher fO_2 in the magma [31,39–42]. As proposed by Ripley and Li [31], a rise in fO_2 , caused by an increase in the H_2O -content of the magma changes the oxidation state of Fe from Fe^{2+} to Fe^{3+} , based on the reaction:



This reaction causes a decrease in the effective Fe^{2+} content and thereby increases the solubility of sulfur [34]. Therefore, the formation of Fe_2O_3 during magmatic crystallization is indicative of high ambient $f\text{O}_2$. However, continued fractional separation of Fe_2O_3 from the magma eventually increases the relative concentration of FeO and decreases the solubility of sulfur. Sulfide liquid saturation can then be attained.

Sulfur content at sulfide saturation (SCSS) is the amount of sulfur at the time of attainment of sulfide liquid saturation in the magma [31,43]. During crystallization, the lowering of temperature decreases the solubility of sulfur and thereby lowers the value of SCSS. However, as explained above, an increase in $f\text{O}_2$ of the magma, as indicated by an increase in the Fe_2O_3 content of the crystallized minerals, can increase the SCSS substantially [44–47], and thereby prevent sulfide liquid saturation.

Conversely, a decrease in SCSS, caused by a sudden drop in $f\text{O}_2$, can induce sulfide liquid saturation and consequently can cause the separation of tiny droplets of sulfide liquid from the magma. In this case, the determinative factor for sulfide liquid separation could be the crystallization of large quantities of oxide phases, such as titaniferous magnetite and ilmenite from the magma. The separation by fractional crystallization of Fe^{3+} and Ti-oxide phases from the magma can thus reduce the SCSS, cause sulfide liquid saturation, and a rapid separation of sulfide liquid from the magma. As proposed by O'Neill and Mavrogenes [46], the excess sulfur displaces O^{2-} anions that bond with Fe^{2+} and forms a Fe-rich immiscible sulfide liquid as seen in the reaction:



4.2. Layered and Conduit-Type Intrusions Associated with the MCR

In the MCR-related layered intrusions of northern Minnesota, PGE mineralization is hosted within sulfide-bearing horizons in troctolitic and gabbroic rocks [3,9,48]. In the Sonju Lake intrusion, PGE and Au mineralization has been reported from an Fe-Ti oxide rich gabbro unit [11]. Sulfide liquid saturation was reached after ~60% crystallization of magma by slow cooling in a closed system [8], possibly triggered by events of devolatilization and decompression.

Cu and PGE are mostly incompatible during crystallization of silicate minerals and thus, the concentrations of these metals increased in the differentiated liquid of a closed system. When the immiscible sulfide liquid formed upon sulfide liquid saturation, Cu, Pt, and Pd partitioned into the sulfide liquid and upon crystallization, the sulfide liquid formed disseminated Cu-Pt-Pd rich grains in the oxide-rich gabbro layer [11]. In the Partridge River and South Kawishiwi intrusions, disseminated sulfide mineralizations of Cu and PGE are found within sheet like units of gabbro and troctolite, which were formed by fractional crystallizations of high-Al olivine tholeiitic (HOAT) parental magmas [5,31,49].

This mineralization-type is in striking contrast with the high-grade Ni, Cu-rich but PGE-poor, sulfide-rich deposits of the Eagle and Tamarack intrusions [13,16]. These deposits have been classified as conduit-type sulfide deposits, where the mineralization occurred during continuous upward movements of magmatic pulses from mantle source-rocks. Supply of external sulfur was critical to the formation of the high-grade, massive, semi-massive, and disseminated mineralizations observed in these intrusions [5]. During magmatic uplift, mineral fractionation was accompanied by crustal contamination and the sulfide liquid saturation of magma was caused by selective assimilation of sulfur-rich Paleoproterozoic meta-sedimentary country rocks the of Michigamme Formation and Upper Thomson Formation for the Eagle deposit and Tamarack deposit, respectively [32,33]. Sulfur-contribution from deeper Neoproterozoic granite-greenstone rocks has also been proposed by the above authors. The overall funnel-shaped cross-sections, as determined by drill-core studies of both intrusions, provide additional evidence for the proposed dynamic conduit-system models. Metallic upgrading, caused by the interaction of accumulated sulfide liquid in the magma conduit, with continuous upheaval of large volumes of metal-enriched magma [50,51], might also have contributed to the high ore-grades of these deposits. Crystallization modeling on high-FeO picritic basalt parental

magmas for the Eagle [32] and Tamarack [33] deposits indicate that the magmas attained sulfide liquid saturation at about 17% crystallization [31]. Separation of sulfide liquid from magma early in the crystallization sequence caused the sulfide liquid to be Ni-rich. In contrast, in the case of late sulfide liquid saturation, the magma is considerably depleted in Ni by the fractional separation of olivine [52].

4.3. Implications from Echo Lake Intrusion

The Echo Lake intrusion is primarily composed of a layered sequence of troctolite, olivine gabbro, and peridotite (Figure 5). The occurrence of a Cu-PGE rich disseminated sulfide horizon in close association with a zone rich in Fe-Ti oxide hosted within olivine gabbro (Figures 5–7), poses a remarkable similarity not only with the Sonju Lake intrusion [8,11] in the MCR, but also with several other layered igneous complexes around the world, such as the Skaergaard Complex [39], southeastern Greenland, the Stella layered intrusion, South Africa [40], the Muskoxt intrusion, Nunavut, Canada [53], and the Kivakka layered intrusion, Russia [54]. PGE-sulfide deposits in these group of intrusions have been classified as “Skaergaard-type” deposits [53].

The variations of chemical proxies such as MgO, TiO₂, Cr₂O₃, and FeO (total) are shown in Figure 8. Strong positive correlations between Pt, Pd, and Cu enrichment in the layered intervals with high TiO₂- and Cr₂O₃-contents can clearly be observed. These are indicators of the peak concentrations of ilmenite and Ti- and Cr-rich magnetite (Table 4) in the mineralized intervals. Since the layered succession is primarily composed of olivine-rich rocks, there is no specific connection between the MgO content and the contents of PGE and Cu. The same is true for FeO (total), and postcumulus titaniferous magnetite is common in several horizons in the layered succession (Figures 3 and 4).

The lithological succession of the Echo Lake intrusion is similar to tholeiitic layered intrusions such as the Skaergaard Complex. The mechanism of PGE-enrichment in the Echo Lake intrusion is consistent with the attainment of sulfide-melt saturation in a high-Al olivine tholeiite (HAOT) magma by fractional crystallization in a closed system [5,8]. The HAOT magmatic composition has been reported from the South Kawishiwi intrusion of the Duluth Complex [55]. This magma is characterized by approximately 20 wt. % Al₂O₃, 7 wt. % MgO and 11 wt. % FeO. Ripley et al. [49] calculated that closed system crystallization of a HAOT magma can produce 17 wt. % olivine (Fo₅₆), 63 wt. % plagioclase (An₆₀), and 14 wt. % clinopyroxene (Mg# 57). This explains the origin of troctolites and olivine gabbros. This model of fractional crystallization in a closed system is in stark contrast to conduit-type, dynamic, open-systems argued for the Eagle and Tamarack intrusions [32,33].

As proposed by Ripley and Li [31], the HAOT magmas could form by fractional crystallization of a more primitive magma, such as a picritic basalt. This implies that the parental magma of the Echo Lake intrusion could potentially be a differentiated liquid from a more primitive magma. This clearly establishes a connection between the open system conduit-type magmatism and the closed system staging-chamber type magmatism associated with the Midcontinent Rift. This is consistent with the proposition that the predominant magma during early magmatism of the Midcontinent Rift was a low-Al, high-FeO picrite, while in the later stages, a well differentiated HAOT magma became prevalent [56]. Peridotites and olivine gabbros reported from the Eagle and Tamarack intrusions show more Mg-rich olivine compositions in the range of Fo_{75–85} [13] and Fo_{82–89} [16], respectively. However, at the Echo Lake intrusion, in troctolite, olivine gabbro, and magnetite-bearing olivine gabbro, the compositional range of olivine is Fo_{57–62} (Table 2). For plagioclase, the compositional range is An_{55–75} (Table 4). These compositions indicate a well-differentiated nature of the parental magma for the Echo Lake intrusion, similar to that reported for the Sonju Lake intrusion [8,11,56]. It is possible that at deeper undiscovered levels of the Echo Lake intrusion, there are peridotite layers with more primitive olivine and plagioclase compositions representative of early crystallization from an undifferentiated magma. An alternating layered succession of this type with dunite, peridotite, and pyroxenite have been reported from intrusions such as the Pados-Tundra ultramafic complex in Kola Peninsula, Russia [57].

Owing to the highly incompatible nature of PGE in silicate minerals, the concentrations of these metals in the magma increases by progressive fractional crystallization in a closed system. However, in an open system, the periodic influx of new magma could reduce the concentration of PGE in the mixed magma. Moreover, in an open system, crustal assimilation and mixing with siliceous magmas could potentially induce sulfide-melt saturation. This could lead to the separation of small batches of immiscible sulfide liquid, which could severely deplete the PGE content of the magma.

However, if sulfide-melt saturation is eventually reached at an advanced stage of magmatic crystallization by the consequent lowering of SCSS [31], PGE can accumulate within the immiscible sulfide liquid. Owing to the increased concentration of PGE in the evolved magma, the separated sulfide liquid, although small in volume, would be extremely enriched in PGE.

Combining all the available evidence from the layered lithological succession, variation trends of chemical constituents, and the localized abundances of chalcophile elements at the Echo Lake intrusion, and comparing these observations with the known reef-type PGE mineralizations in layered intrusions of MCR and around the world, the following mechanism of mineralization can be argued for the Echo Lake deposit. A HAOT-type magma [58] began crystallizing olivine, plagioclase, and relatively small quantities of pyroxene. The early crystallized olivine (Fo₆₂) and plagioclase (An₇₄) formed a cumulus mosaic texture with small grains of clinopyroxene in fine interstitial spaces. This caused the large observed volumetric abundances of troctolite and anorthosite in the layered sequence. Early crystallization of plagioclase enriched the magma in FeO. Crystallizations of olivine (Fo_{57–62}) and small proportions of augite lowered the FeO content slightly. Overall, the FeO-content of the magma increased steadily with fractional crystallization. This was accompanied by a progressive rise of H₂O and *f*O₂ in the magma. At an advanced stage in magmatic differentiation, a threshold point was reached, when the magma became super-saturated in FeO and this led to the crystallization of titaniferous magnetite, accompanied by ilmenite and chromite. Rapid precipitation of large quantities of oxide minerals created local zones of sulfide-melt saturation and the formation of disseminated Cu, PGE-enriched sulfide minerals. The highest concentrations of Cu and PGE are hosted within a Fe-Ti oxide rich layer of gabbro with disseminated sulfide minerals, between depths of 990 and 1010 m. It is possible that this mineralized interval was emplaced within the stratigraphic sequence by an H₂O-rich magmatic pulse mobilized from a separate part of the magma chamber.

The heightened abundances of oxide minerals are obvious indicators of high *f*O₂, which separated Fe as Fe³⁺ and thereby suddenly lowered the effective concentration of FeO in the melt. This caused localized zones of sulfide liquid saturation and the formation of tiny droplets of immiscible sulfide liquid. These immiscible droplets formed in isolated pockets, sequestered the chalcophile elements such as Pd, Pt, and Cu from the surrounding melt, and eventually crystallized to form the disseminated sulfide mineralized horizon. Isolated and small occurrences of delicate titaniferous magnetite-sulfide intergrowths and thin sulfide rims around larger titaniferous magnetite grain-boundaries (Figure 4) imply close relationships between the crystallizations of titaniferous magnetite and sulfide minerals like chalcopyrite. Local occurrences of biotite- titaniferous magnetite intergrowths (Figure 4) provide evidence of pockets of intercumulus melt enriched in H₂O.

In the complete layered interval, the concentration peaks for Pt and Pd overlap with each other, but the peak for Cu does not (Figures 5–7). This stratigraphic offset of concentration peaks has been reported from other layered-type sulfide deposits, such as the Sonju Lake intrusion [12], Skaergaard Complex [39], and the Bushveld Complex [59], and has been explained by differences in liquid/silicate partitioning coefficients for chalcophile metals, or by the fractionation of sulfide melt during compaction of layered successions of cumulates [40]. The low abundance of Ni in this mineralized sulfide interval can be explained by the depletion of Ni in the magma, caused by the large fractionation of olivine early in the crystallization history.

Discovery of the PGE-Cu enriched mineralized zone in the Echo Lake intrusion is significant for many reasons. This deposit shares several important characteristics with the layered PGE-rich units of the Duluth and Beaver Bay complexes, as inferred in this study. Although the reported

observations in this study are based on a limited dataset generated from preliminary exploratory studies, the implications of these findings are profound and are indicative of potential reef-type PGE-mineralizations in layered mafic-ultramafic sequences in other parts of the Midcontinent Rift region, apart from the well-known layered intrusions in northern Minnesota.

Author Contributions: A.J.K. collected samples, generated data and wrote an initial draft of manuscript. J.T. supervised the project and wrote the final manuscript.

Funding: This research was funded by Altius Resources Inc. grant number 9622.

Acknowledgments: This study was performed with the support and assistance of Altius Minerals Inc. and Bitterroot Resources. We especially thank Michael Carr of Bitterroot Resources and Roderick Smith of Altius Minerals for giving us access to the drill core samples, core data, and for their useful comments during all phases of this work. Several people, including Melanie Humphrey from the Department of Environmental Quality, Michigan, and Nick Moleski from Western Michigan University, helped us to collect drill core samples. Comments from two anonymous reviewers and useful suggestions by the editor helped us to improve the quality of this manuscript. Peter Voice, Robb Gillespie, and R.V. Krishnamurthy provided feedback in early stages of this work.

Conflicts of Interest: The authors declare no conflict of interest. The funders provided access to samples and core data. The funders had no role in the design of the study; in the interpretation of data; in the writing of the manuscript, or in the decision to publish the results.

References

1. Nicholson, S.W.; Shirey, S.B.; Schulz, K.J.; Green, J.C. Rift-wide correlation of 1.1 Ga Midcontinent rift system basalts: Implications for multiple mantle sources during rift development. *Can. J. Earth Sci.* **1997**, *34*, 504–520. [[CrossRef](#)]
2. Hauck, S.; Severson, M.J.; Zanko, L.M.; Barnes, S.-J.; Morton, P.; Alminas, H.V.; Foord, E.E.; Dahlberg, E.H. An overview of the geology and oxide, sulfide, and platinum-group element mineralization along the western and northern contacts of the Duluth Complex. *Spec. Pap. Geol. Soc. Am.* **1997**, *312*, 137–185. [[CrossRef](#)]
3. Severson, M.J.; Miller, J.D., Jr.; Peterson, D.M.; Green, J.C.; Hauck, S.A. Mineral Potential of the Duluth Complex and related intrusions. In *RI-58 Geology and Mineral Potential of the Duluth Complex and Related Rocks of Northeastern Minnesota*; Minnesota Geological Survey Report of Investigations; Miller, J.D., Jr., Green, J.C., Severson, M.J., Chandler, V.W., Hauck, S.A., Peterson, D.M., Wahl, T.E., Eds.; Minnesota Geological Survey: Saint Paul, MN, USA, 2002; pp. 164–200.
4. Ripley, E.M.; Li, C. Ni-Cu-PGE mineralization associated with the Proterozoic Midcontinent rift system, USA. In *New Developments in Magmatic Ni-Cu and PGE Deposits*; Li, C., Ripley, E.M., Eds.; Geological Publishing House: Beijing, China, 2009; pp. 180–191.
5. Ripley, E.M. Ni-Cu-PGE Mineralization in the Partridge River, South Kawishiwi, and Eagle Intrusions: A Review of Contrasting Styles of Sulfide-Rich Occurrences in the Midcontinent Rift System. *Econ. Geol.* **2014**, *109*, 309–324. [[CrossRef](#)]
6. Miller, J.; Nicholson, S. Geology and mineral deposits of the 1.1 Ga midcontinent rift in the Lake Superior region—An overview. Field guide to copper-nickel-platinum group element deposits of the Lake Superior region. *Precambrian Res. Center Guideb.* **2013**, *13–01*, 1–49.
7. Altius Minerals. *Voyageur Lands—Michigan: Project Summary. 2015 Technical Report for Summary of Project Area*; Altius Minerals: St. John's, NL, Canada, 2015; pp. 1–9.
8. Miller, J.D., Jr.; Ripley, E.M. Layered Intrusion of the Duluth Complex, Minnesota, USA. In *Layered Intrusions*; Cawthorn, R.G., Ed.; Elsevier Scientific: Amsterdam, The Netherlands, 1996; pp. 257–301.
9. Miller, J.D., Jr.; Green, J.C.; Severson, M.J.; Chandler, V.W.; Hauck, S.A.; Peterson, D.M.; Wahl, T.E. *RI-58 Geology and Mineral Potential of the Duluth Complex and Related Rocks of Northeastern Minnesota*; Minnesota Geological Survey Report of Investigations; Minnesota Geological Survey: Saint Paul, MN, USA, 2002; 207p.
10. Paces, J.B.; Miller, J.D. Precise U-Pb ages of Duluth Complex and related mafic intrusions, northeastern Minnesota: Geochronological insights into physical, petrogenetic, paleomagnetic, and tectonomagnetic processes associated with the 1.1 Ga Midcontinent rift system. *J. Geophys. Res.* **1993**, *98*, 13997–14013. [[CrossRef](#)]
11. Miller, J.D., Jr. *Information Circular 44. Geochemical Evaluation of Platinum Group Element (PGE) mineralization in the Sonju Lake Intrusion, Finland, Minnesota*; Minnesota Geological Survey: Saint Paul, MN, USA, 1999; 32p.

12. Joslin, G.J. Stratiform Palladium-Platinum-Gold Mineralization in the Sonju Lake Intrusion, Lake County, Minnesota. Master's Thesis, University of Minnesota Duluth, Duluth, MN, USA, 2004.
13. Ding, X.; Li, C.; Ripley, E.M.; Rossell, D.; Kamo, S. The Eagle and East Eagle sulfide ore-bearing mafic-ultramafic intrusions in the Midcontinent Rift System, upper Michigan: Geochronology and petrologic evolution. *Geochem. Geophys. Geosyst.* **2010**, *11*, Q03003. [[CrossRef](#)]
14. Goldner, B.D. Igneous Petrology of the Ni-Cu-PGE Mineralized Tamarack Intrusion, Aitkin and Carlton Counties, Minnesota. Master's Thesis, University of Minnesota Duluth, Duluth, MN, USA, 2011.
15. Keays, R.R.; Lightfoot, P.C. Geochemical Stratigraphy of the Keweenaw Midcontinent Rift Volcanic Rocks with Regional Implications for the Genesis of Associated Ni, Cu, Co, and Platinum Group Element Sulfide Mineralization. *Econ. Geol.* **2015**, *110*, 1235–1267. [[CrossRef](#)]
16. Taranovic, V.; Ripley, E.M.; Li, C.; Rossell, D. Petrogenesis of the Ni-Cu-PGE sulfide bearing Tamarack Intrusive Complex, Midcontinent Rift System, Minnesota. *Lithos* **2015**, *212–215*, 16–31. [[CrossRef](#)]
17. Sims, P.K. *Geologic Map of Precambrian Rocks, Southern Lake Superior Region, Wisconsin and Northern Michigan*; U.S. Geological Survey Miscellaneous Investigations Map I-2185; USGS: Reston, VA, USA, 1992.
18. Bitterroot Resources Ltd. *Echo Lake Ni/Cu/PGE Project: Upper Peninsula of Michigan*; 1999 Technical Report on Summary of Project Area; Bitterroot Resources Ltd.: West Vancouver, BC, Canada, 1999; pp. 1–26.
19. Peterman, Z.E.; Zartman, R.E.; Sims, P.K. A protracted Archean history in the Watersmeet gneiss dome, northern Michigan. In *Shorter Contributions to Isotope Research*; Peterman, Z.E., Schnabel, D.C., Eds.; U.S. Geological Survey Bulletin: Reston, VA, USA, 1986; Volume 1622, pp. 51–64.
20. Van Schmus, W.R.; Bickford, M.E.L.; Zietz, I. Early and middle Proterozoic provinces in the central United States. In *Proterozoic Lithosphere Evolution*; Geodynamics Series; Kroner, A., Ed.; AGU: Washington, DC, USA, 1987; Volume 17, pp. 43–68.
21. Malone, D.H.; Stein, C.A.; Craddock, J.P.; Kley, J.; Stein, S.; Malone, J.E. Maximum depositional age of the Neoproterozoic Jacobsville Sandstone, Michigan: Implications for the evolution of the Midcontinent Rift. *Geosphere* **2016**, *12*, 1271–1282. [[CrossRef](#)]
22. Koerber, A. Geochemical and Petrological Investigation of the Prospective Ni-Cu-PGE Mineralization at the Echo Lake Intrusion in the Upper Peninsula of Michigan, USA. Master's Thesis, Western Michigan University, Kalamazoo, MI, USA, 2018.
23. Cannon, W.F.; Nicholson, S.W. *Geologic Map of the Keweenaw Peninsula and adjacent Area*; Michigan U.S. Geological Survey Miscellaneous Investigations Map I-2696; USGS: Reston, VA, USA, 2001.
24. Barnes, S.-J.; Maier, W.D. Platinum group elements and microstructures of normal Merensky Reef from Impala platinum mines, Bushveld Complex. *J. Petrol.* **2002**, *43*, 103–128. [[CrossRef](#)]
25. Campbell, I.H.; Naldrett, A.J.; Barnes, S.J. A model for the origin of the platinum-rich sulfide horizons in the Bushveld and Stillwater Complexes. *J. Petrol.* **1983**, *24*, 133–165. [[CrossRef](#)]
26. Boudreau, A.E.; Mathez, E.A.; McCallum, I.S. Halogen geochemistry of the Stillwater and Bushveld complexes: Evidence for transport of the platinum-group elements by Cl-rich fluids. *J. Petrol.* **1986**, *27*, 967–986. [[CrossRef](#)]
27. Donovan, J.J.; Tingle, T.N. An improved mean atomic number correction for quantitative microanalysis. *Microsc. Microanal.* **1996**, *2*, 1–7. [[CrossRef](#)]
28. Ripley, E.M.; Li, C. Sulfur isotopic exchange in the formation of magmatic Cu-Ni-(PGE) deposits. *Econ. Geol.* **2003**, *98*, 635–641. [[CrossRef](#)]
29. Seat, Z.; Beresford, S.W.; Grguric, B.A.; Mary Gee, M.A.; Grassineau, N.V. Reevaluation of the Role of External Sulfur Addition in the Genesis of Ni-Cu-PGE Deposits: Evidence from the Nebo-Babel Ni-Cu-PGE Deposit, West Musgrave, Western Australia. *Econ. Geol.* **2009**, *104*, 521–538. [[CrossRef](#)]
30. Keays, R.R.; Lightfoot, P.C. Crustal sulfur is required to form magmatic Ni-Cu sulfide deposits: Evidence from chalcophile element signatures of Siberian and Deccan Trap basalts. *Miner. Deposita* **2010**, *45*, 241–257. [[CrossRef](#)]
31. Ripley, E.M.; Li, C. Sulfide saturation in mafic magmas: Is external sulfur required for magmatic Ni-Cu-(PGE) ore genesis? *Econ. Geol.* **2013**, *108*, 45–58. [[CrossRef](#)]
32. Ding, X.; Ripley, E.M.; Shirey, S.B.; Li, C. Os, Nd, O and S isotope constraints on country rock contamination in the conduit-related Eagle Cu-Ni-(PGE) deposit, Midcontinent rift system, upper Michigan. *Geochim. Cosmochim. Acta* **2012**, *89*, 10–30. [[CrossRef](#)]

33. Taranovic, V.; Ripley, E.M.; Li, C.; Shirey, S.B. S, O, and Re-Os Isotope Studies of the Tamarack Igneous Complex: Melt-Rock Interaction During the Early Stage of Midcontinent Rift Development. *Econ. Geol.* **2018**, *113*, 1161–1179. [[CrossRef](#)]
34. Lehmann, J.; Arndt, N.; Windley, B.; Zhou, M.-F.; Wang, C.Y.; Harris, C. Field relationships and geochemical constraints on the emplacement of the Jinchuan intrusion and its Ni-Cu-PGE sulfide deposit, Gansu, China. *Econ. Geol.* **2007**, *102*, 75–94. [[CrossRef](#)]
35. Holwell, D.A.; Boyce, A.J.; McDonald, I. Sulfur isotope variations within the Platreef Ni-Cu-PGE deposit: Genetic implications for the origin of sulfide mineralization. *Econ. Geol.* **2007**, *102*, 1091–1110. [[CrossRef](#)]
36. Howarth, G.H.; Prevec, S.A. Trace element, PGE, and Sr–Nd isotope geochemistry of the Panzhihua mafic layered intrusion, SW China: Constraints on ore-forming processes and evolution of parent magma at depth in a plumbing-system. *Geochim. Cosmochim. Acta* **2013**, *120*, 459–478. [[CrossRef](#)]
37. Carmichael, I.S.E. The redox states of basic and silicic magmas: A reflection of their source regions? *Contrib. Mineral. Petrol.* **1991**, *106*, 129–141. [[CrossRef](#)]
38. Liu, Y.; Samaha, N.T.; Baker, D.R. Sulfur concentration at sulfide saturation (SCSS) in magmatic silicate melts. *Geochim. Cosmochim. Acta* **2007**, *71*, 1783–1799. [[CrossRef](#)]
39. Andersen, J.C.O.; Rasmussen, H.; Neilsen, T.F.D.; Ronsbo, J.G. The Triple Group and the Platinova gold and palladium reefs in the Skaergaard intrusion: Stratigraphic and petrographic relations. *Econ. Geol.* **1998**, *93*, 488–509. [[CrossRef](#)]
40. Maier, W.D.; Barnes, S.-J.; Gartz, V.; Andrews, G. Pt-Pd reefs in magnetites of the Stella layered intrusion, South Africa: A world of new exploration opportunities for platinum group elements. *Geology* **2003**, *31*, 885–888. [[CrossRef](#)]
41. Kelley, K.A.; Cottrell, E. The influence of magmatic differentiation on the oxidation state of Fe in a basaltic arc magma. *Earth Planet. Sci. Lett.* **2012**, *329–330*, 109–121. [[CrossRef](#)]
42. Holwell, D.A.; Keays, R.R. The Formation of Low-Volume, High-Tenor Magmatic PGE-Au Sulfide Mineralization in Closed Systems: Evidence from Precious and Base Metal Geochemistry of the Platinova Reef, Skaergaard Intrusion, East Greenland. *Econ. Geol.* **2014**, *109*, 387–406. [[CrossRef](#)]
43. Li, C.; Ripley, E.M. Sulfur contents at sulfide-liquid or anhydrite saturation in silicate melts: Empirical equations and example applications. *Econ. Geol.* **2009**, *104*, 405–412. [[CrossRef](#)]
44. Gaetani, G.A.; Grove, T.L. Partitioning of moderately siderophile elements among olivine, silicate melt, and sulfide melt: Constraints on core formation in the Earth and Mars. *Geochim. Cosmochim. Acta* **1997**, *61*, 1829–1846. [[CrossRef](#)]
45. Carroll, M.R.; Rutherford, M.J. Sulfur speciation in hydrous experimental glasses of varying oxidation state: Results from measured wavelength shifts of sulfur X-rays. *Am. Miner.* **1988**, *73*, 845–849.
46. O'Neill, H.St.C.; Mavrogenes, J.A. The sulfide capacity and the sulfur content at sulfide saturation of silicate melts at 1400°C and 1 bar. *J. Petrol.* **2002**, *43*, 1048–1087.
47. Jugo, P.J.; Luth, R.W.; Richards, J.P. Experimental data on the speciation of sulfur as a function of oxygen fugacity in basaltic melts. *Geochim. Cosmochim. Acta* **2005**, *69*, 497–503. [[CrossRef](#)]
48. Theriault, R.D.; Barnes, S.-J.; Severson, M.J. Origin of Cu-Ni-PGE sulfide mineralization in the Partridge River intrusion, Duluth Complex, Minnesota. *Econ. Geol.* **2000**, *95*, 929–944. [[CrossRef](#)]
49. Ripley, E.M.; Taib, N.I.; Li, C.; Moore, C.H. Chemical and mineralogical heterogeneity in the basal zone of the Partridge River Intrusion: Implications for the origin of Cu-Ni mineralization in the Duluth Complex, Midcontinent rift system. *Contrib. Mineral. Petrol.* **2007**, *154*, 35–54. [[CrossRef](#)]
50. Naldrett, A.J. World-class Ni-Cu-PGE deposits; key factors in their genesis. *Miner. Deposita* **1999**, *34*, 227–240. [[CrossRef](#)]
51. Li, C.; Ripley, E.M.; Naldrett, A.J. Compositional variation of olivine and sulfur isotopes in the Noril'sk and Talnakh intrusions, Siberia: Implications for ore-forming processes in dynamic magma conduits. *Econ. Geol.* **2003**, *98*, 69–86. [[CrossRef](#)]
52. Barnes, S.-J.; Francis, D. The distribution of platinum-group elements, nickel, copper, and gold in the Muskox layered intrusion, Northwest Territories, Canada. *Econ. Geol.* **1995**, *90*, 135–154. [[CrossRef](#)]
53. Miller, J.D., Jr.; Andersen, J.C.O. Attributes of Skaergaard-type PGE deposits [abs.]. In Proceedings of the 9th International Platinum Symposium, Billings, MT, USA, 21–25 July 2002.
54. Barkov, A.Y.; Nikiforov, A.A. Compositional variations of apatite, fractionation trends, and a PGE-bearing zone in the Kivakka layered intrusion, northern Karelia, Russia. *Can. Mineral.* **2016**, *54*, 475–490. [[CrossRef](#)]

55. Lee, I.; Ripley, E.M. Mineralogic and oxygen isotopic studies of open system magmatic processes in the South Kawishiwi intrusion, Spruce Road Area, Duluth Complex, Minnesota. *J. Petrol.* **1996**, *37*, 1437–1461. [[CrossRef](#)]
56. Park, Y.-R.; Ripley, E.M.; Miller, J.D.; Li, C.; Mariga, J.; Shafer, P. Stable isotopic constraints on fluid-rock interaction and Cu-PGE-S redistribution in the Sonju Lake intrusion. *Econ. Geol.* **2004**, *99*, 325–338. [[CrossRef](#)]
57. Barkov, A.Y.; Nikiforov, A.A.; Martin, R.F. The structure and cryptic layering of the Pados-Tundra ultramafic complex, Serpentine belt, Kola Peninsula, Russia. *Bull. Geol. Soc. Finl.* **2017**, *89*, 35–56. [[CrossRef](#)]
58. Li, C.; Ripley, E.M. Empirical equations to predict the sulfur content of mafic magmas at sulfide saturation and applications to magmatic sulfide deposits. *Miner. Deposita* **2005**, *40*, 218–230. [[CrossRef](#)]
59. Maier, W.D.; Barnes, S.-J. Platinum-Group Elements in Silicate Rocks of the Lower, Critical and Main Zones at Union Section, Western Bushveld Complex. *J. Petrol.* **1999**, *40*, 1647–1671. [[CrossRef](#)]



© 2018 by the authors. Licensee MDPI, Basel, Switzerland. This article is an open access article distributed under the terms and conditions of the Creative Commons Attribution (CC BY) license (<http://creativecommons.org/licenses/by/4.0/>).